Abdominal Radiology (2023) 48:1831–1839
https://doi.org/10.1007/s00261-022-03747-3

CORRECTION

Correction: Perinephric myxoid pseudotumor of fat: a multimodality imaging case series

Justin Lee[1] · Kevin G. King[2] · Shefali Chopra[3] · Phillip M. Cheng[4]

Published online: 17 February 2023

Correction to: Abdominal Radiology
https://doi.org/10.1007/s00261-022-03662-7

The original version of this article unfortunately contained a mistake. In particular, the figure part labels were missing, and Figs. 7 and 8 were switched. In the visual abstract, citation information was missing. The corrected figures are provided below.

The original article has been updated.

Graphical abstract

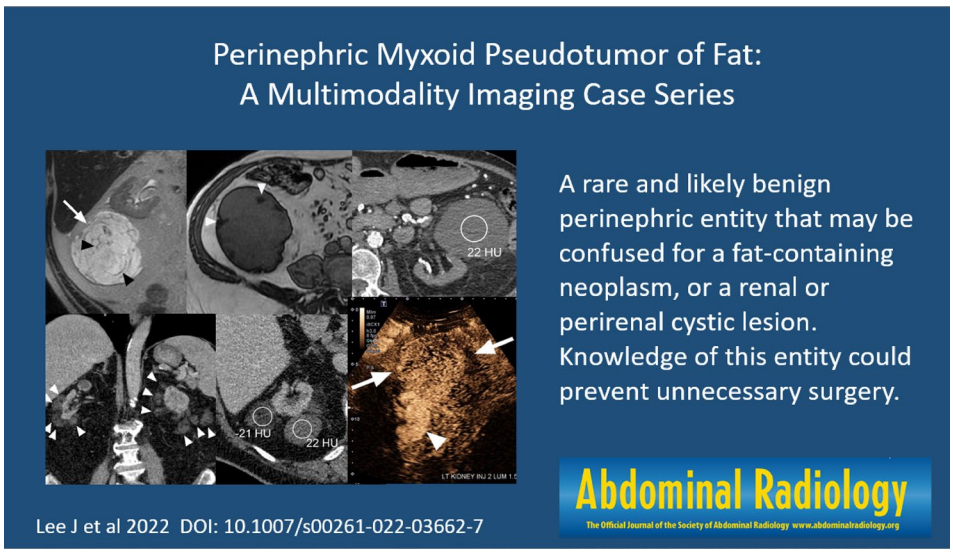

The original article can be found online at https://doi.org/10.1007/s00261-022-03662-7.

✉ Phillip M. Cheng
Phillip.Cheng@med.usc.edu

Justin Lee
Justin.Lee2@med.usc.edu

Kevin G. King
kgking@mednet.ucla.edu

Shefali Chopra
Shefali.Chopra@med.usc.edu

[1] Department of Radiology, Keck School of Medicine of USC, Los Angeles, CA, USA

[2] Department of Radiology, David Geffen School of Medicine at UCLA, Los Angeles, CA, USA

[3] Department of Pathology, Keck School of Medicine of USC, Los Angeles, CA, USA

[4] Department of Radiology, Keck School of Medicine of USC, 1441 Eastlake Ave., Suite 2315B, Los Angeles, CA 90033, USA

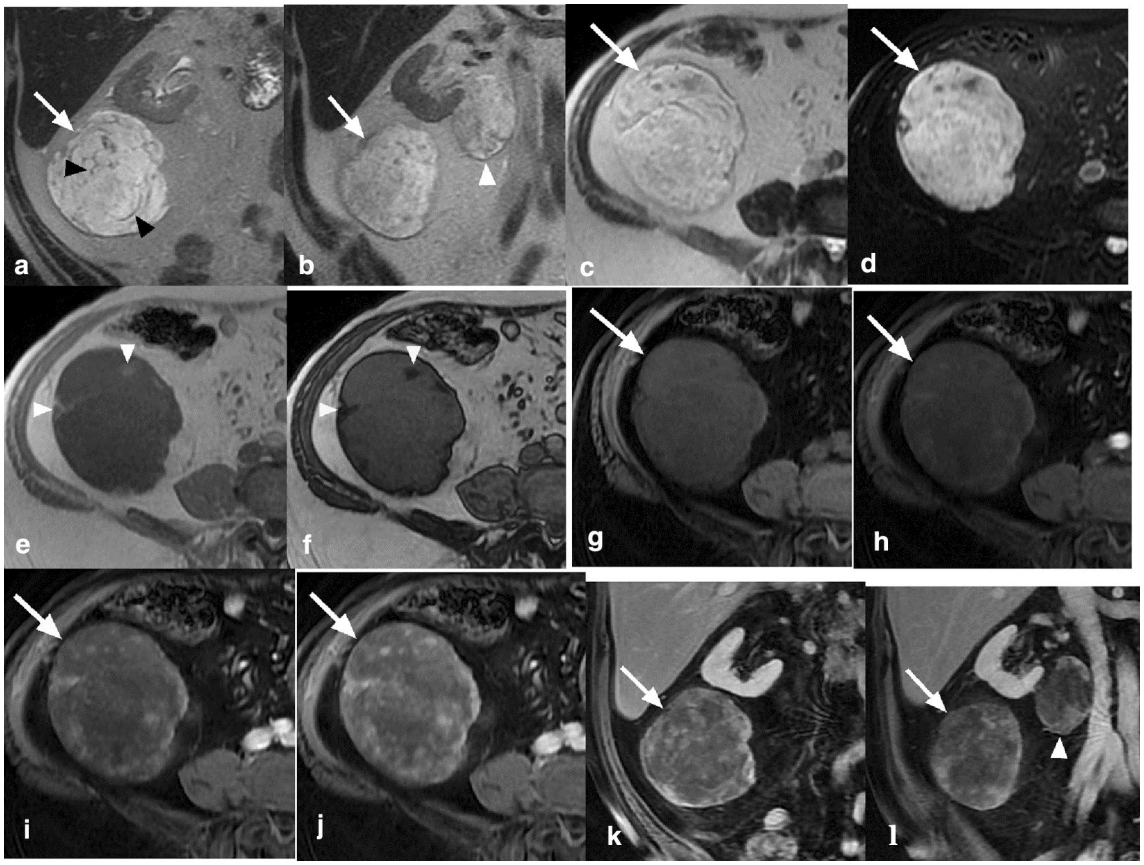

Fig. 1 Axial MRI images at 1.5 T of two right perirenal masses in Case 1. T2-weighted coronal images **a**, **b** demonstrate two perirenal T2 hyperintense masses, the larger inferolateral (white arrows) and the smaller inferomedial (**b**, white arrowhead). There appear to be curvilinear hypointense septations in the masses, more prominent in the larger mass (**a**, black arrowheads). T2-weighted axial images of the larger mass (arrow) without (**c**) and with (**d**) fat saturation similarly show intense T2 hyperintensity. Small peripheral foci of macroscopic fat (arrowheads) within the larger mass are hyperintense on in-phase T1-weighted images (**e**), and hypointense on opposed-phase T1-weighted images (**f**), as they are completely obscured by India ink artifact owing to their small size. T1-weighted fat-saturated axial images without contrast (**g**) and in the arterial phase (**h**), portal venous phase (**i**), and delayed phase (**j**) demonstrate gradual enhancement of the larger mass (arrow). T1-weighted fat-saturated coronal images (**k**, **l**) similarly show enhancement of both the larger (white arrows) and smaller (white arrowhead) masses

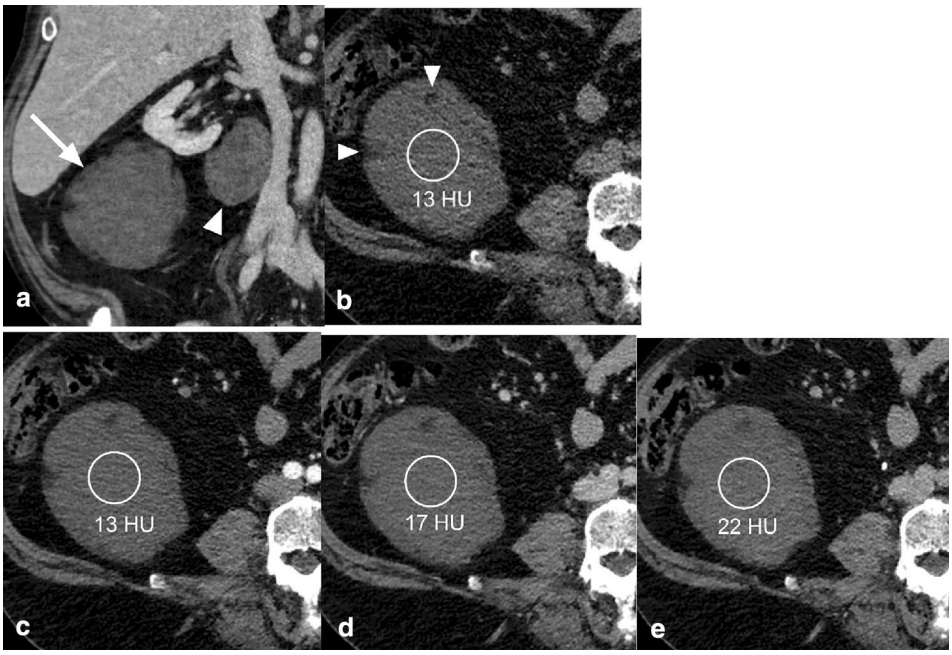

Fig. 2 CT images for Case 1. Coronal nephrographic phase CT image **a** shows two right perinephric hypoattenuating masses, the larger (arrow) inferolateral to the kidney and the smaller (arrowhead) inferomedial to the kidney. Noncontrast axial CT through the larger mass (**b**) shows small peripheral foci of fat attenuation within the mass (arrowheads), while the rest of the lesion measures near water attenuation. No clear enhancement is seen in the mass based on mean attenuation measurements of regions of interest in noncontrast (**b**), corticomedullary (**c**), nephrographic (**d**), and excretory (**e**) phases

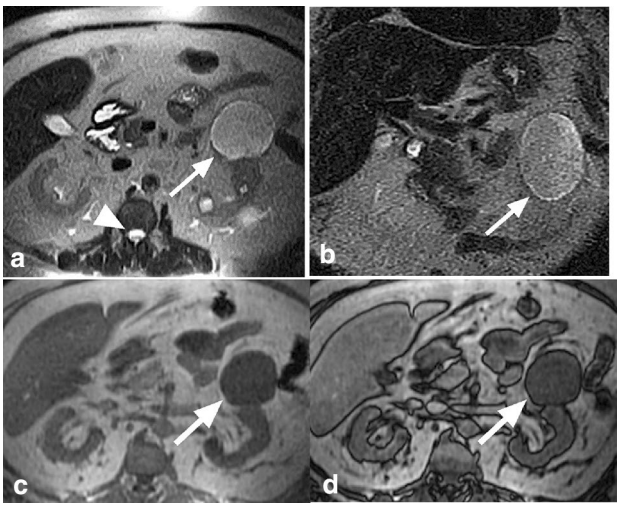

Fig. 3 MRI images at 1.2 T for Case 2 demonstrating atrophied kidneys consistent with end-stage renal disease. Axial (**a**) and coronal (**b**) T2-weighted images of the abdomen demonstrate a T2-hyperintense lesion at the anterior aspect of the left kidney (arrow). Note that the T2 hyperintensity of the mass is less than that of the cerebrospinal fluid (**a**, arrowhead). Axial T1 in-phase (**c**) and out-of-phase (**d**) images did not demonstrate evidence of microscopic or macroscopic fat

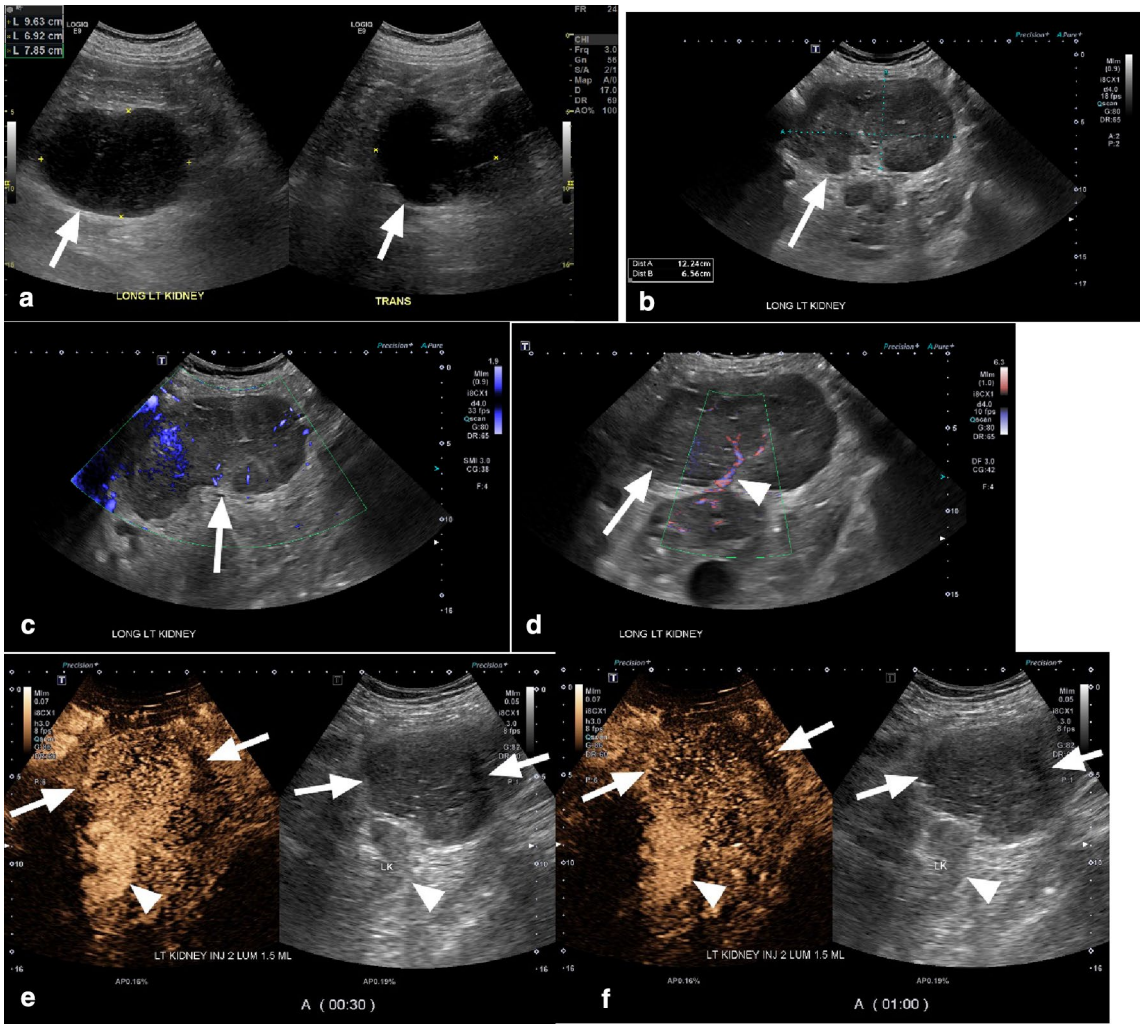

Fig. 4 Sonographic images of the left anterior perirenal mass in Case 2. **a** Longitudinal and transverse greyscale images obtained 1 month after the MRI in Fig. 3 show a lobulated hypoechoic lesion (arrows) with low level internal echoes that was interpreted as a complex cyst. Images **b**–**f** were obtained 2 years later. **b** The mass (arrow) appears solid on greyscale imaging. **c** The mass (arrow) demonstrates internal flow on power Doppler. **d** Color Doppler imaging demonstrates a vessel (arrowhead) extending from the kidney into the mass (arrow). **e**–**f** Contrast-enhanced ultrasound of the mass (arrows) and adjacent kidney (arrowheads). The mass reveals diffuse contrast enhancement at 30 s (**e**) and mild partial washout at 60 s (**f**)

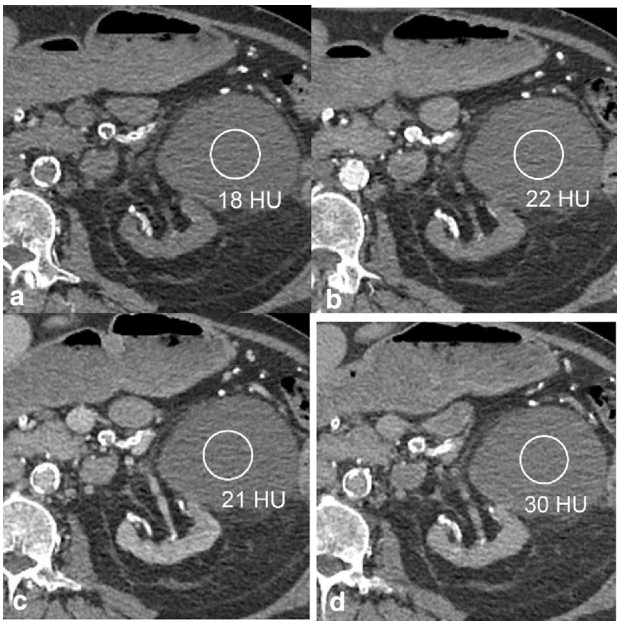

Fig. 5 Multiphase renal CT for the patient in Case 2 with noncontrast (**a**), corticomedullary phase (**b**), nephrographic phase (**c**), and delayed phase (**d**) images. Enhancement was equivocal within the left perirenal lesion

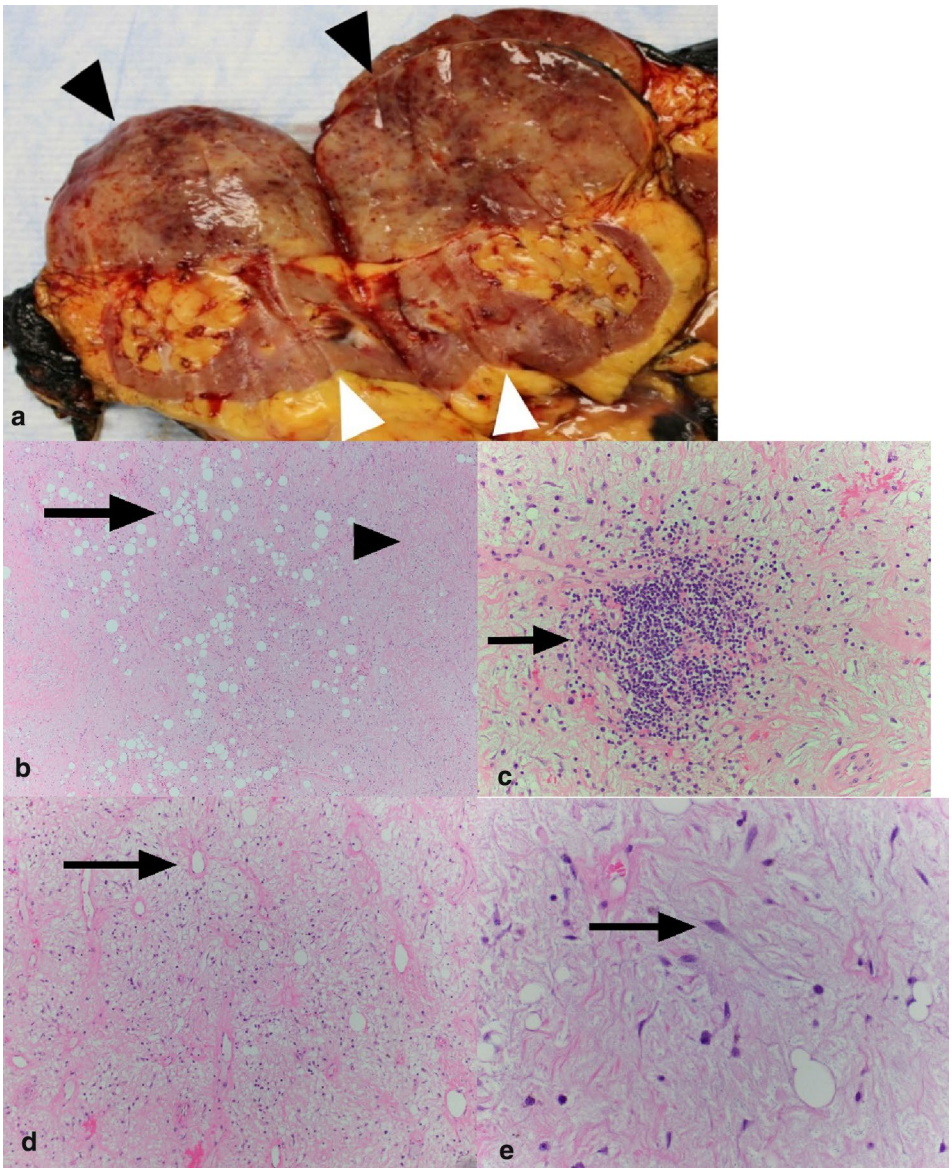

Fig. 6 **a** Gross specimen from case 2 with bivalved mass (black arrowheads) and adjacent left kidney (white arrowheads). **b–e** Histological slides from the mass. **b** (Hematoxylin–eosin [HE] × 40) Admixture of mature fat (arrow), myxoid stroma, and spindled to stellate stromal cells (arrowhead). **c** (HE × 200) Variably intense mixed inflammatory cell infiltrate (arrow) consisting predominantly of lymphocytes. **d** (HE × 100) Well-developed, thick-walled, arborizing vasculature, with one vessel highlighted (arrow). **e** (HE × 400) Stromal and stellate cells containing small nuclei with evenly dispersed chromatin (arrow)

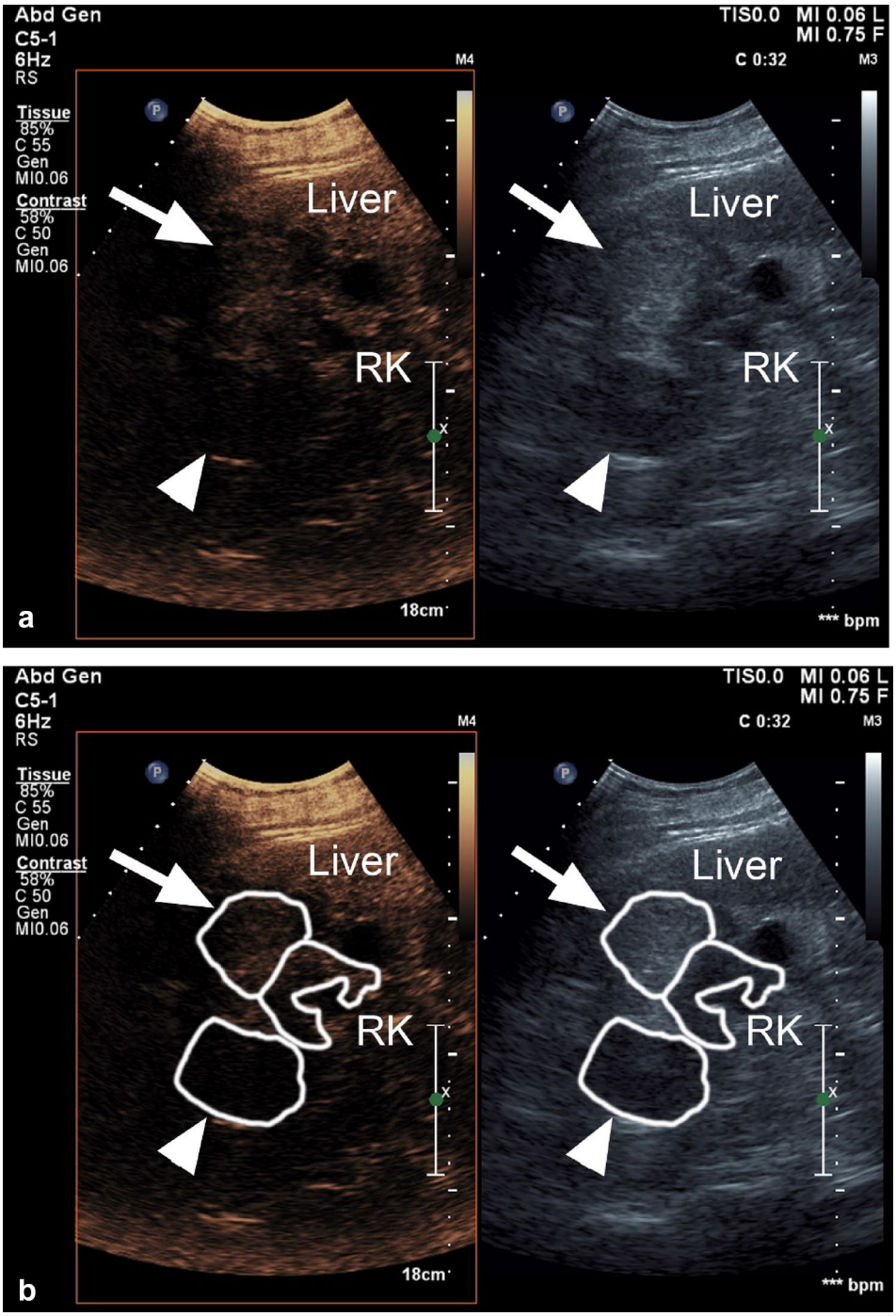

Fig. 7 **a**, **b** Case 3 contrast-enhanced ultrasound images transversely oriented through the upper pole of the right kidney (RK) obtained 32 s after contrast injection; the transducer was placed at the right lateral aspect of the patient. The two largest perinephric lesions, one lateral (arrow) and one medial (arrowhead) are indicated, corresponding to the lesions biopsied in Fig. 8. No clear enhancement was seen in either lesion. **b** shows outlines of the structures indicated in **a**

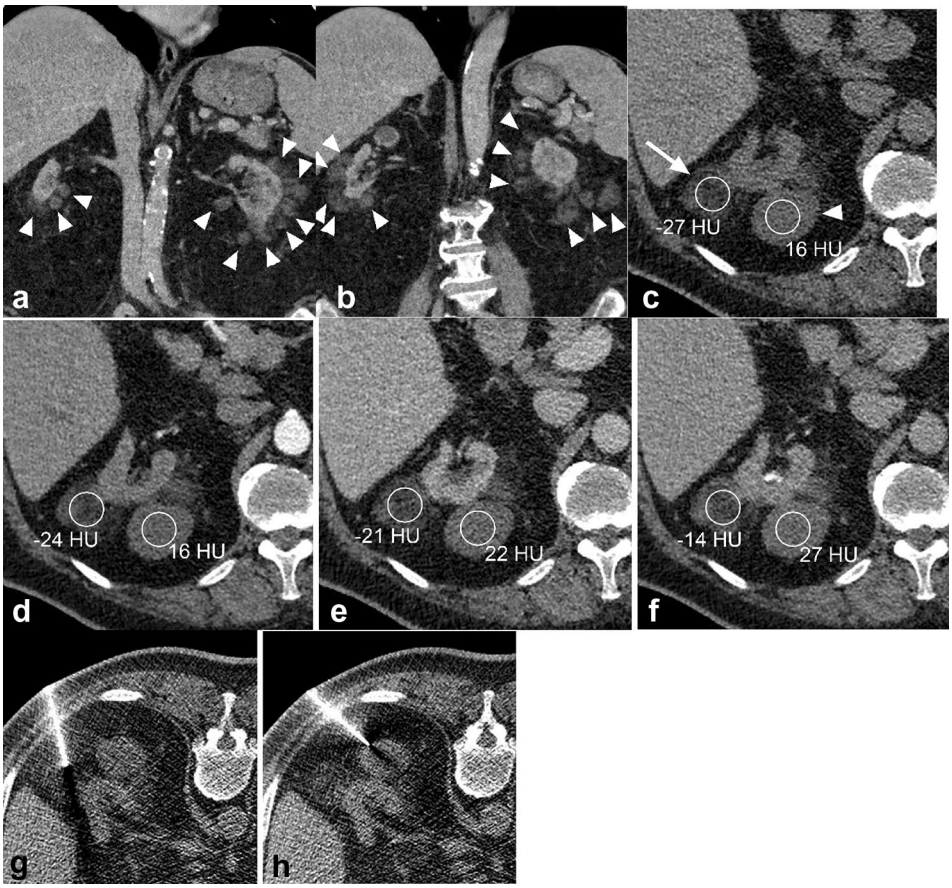

Fig. 8 CT images for Case 3. Coronal nephrographic phase CT images (**a** and **b**) demonstrate numerous bilateral perirenal or exophytic lesions (arrowheads), many ill-defined, with variable attenuation ranging from fat attenuation to slightly higher than water attenuation. **c** Noncontrast axial image demonstrates the two largest lesions along the posterior aspect of the right kidney, with the more lateral lesion (arrow) containing macroscopic fat, and the more medial lesion (arrowhead) slightly higher than water attenuation. Postcontrast corticomedullary (**d**), nephrographic (**e**), and delayed (**f**) phase images show equivocal enhancement in both lesions. **g**, **h** Prone images from CT-guided biopsies of the two lesions in **c**–**f**, which revealed myxoid features in both lesions

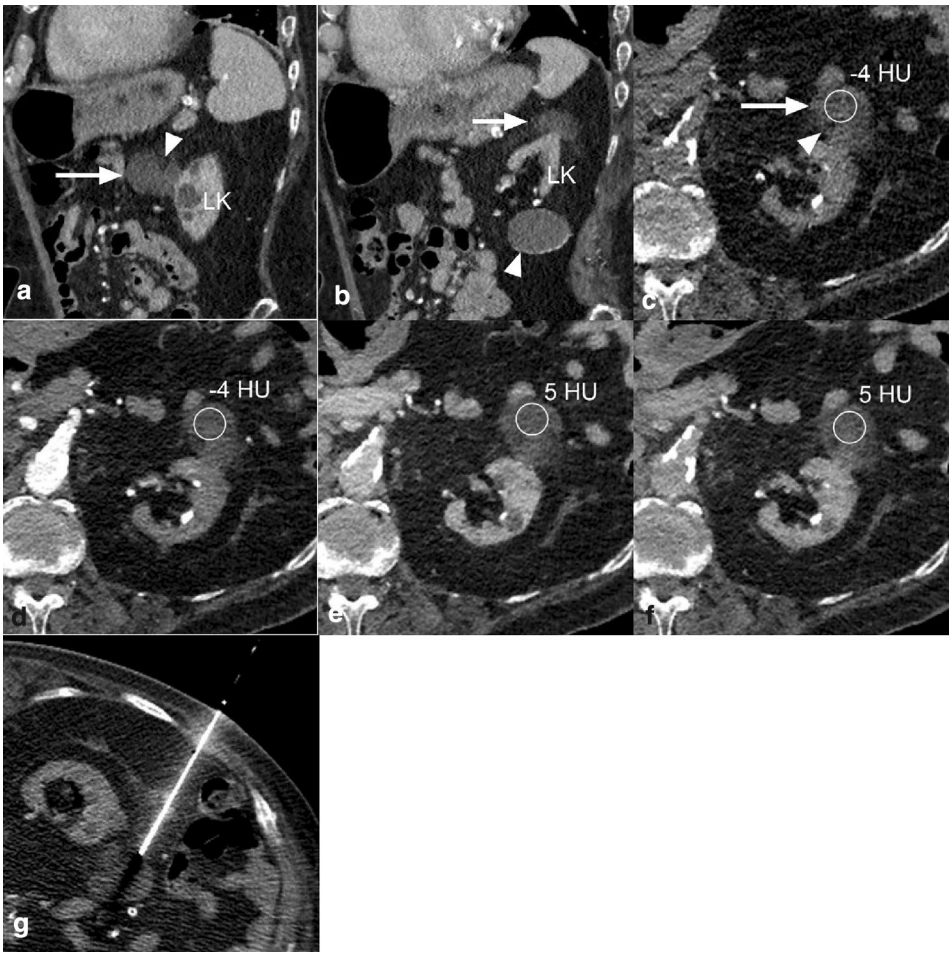

Fig. 9 Case 4 CT images. **a** Sagittal nephrographic phase CT image demonstrating an ill-defined perirenal or exophytic mass (arrow) anterior to the left kidney (LK) containing a focus of macroscopic fat (arrowhead). **b** A more lateral sagittal nephrographic phase image demonstrates a smaller ill-defined perirenal or exophytic mass (arrow) at the superior aspect of the left kidney (LK); a rim-calcified exophytic non-enhancing lesion higher than water attenuation is also seen at the lower pole of the left kidney (arrowhead), compatible with a proteinaceous cyst. **c** Noncontrast image of the larger mass (seen in **a**) demonstrates an ill-defined left anterior perinephric mass, near water attenuation (arrow), containing a focus of macroscopic fat (arrowhead). Postcontrast corticomedullary (**d**), nephrographic (**e**), and delayed (**f**) phases do not demonstrate clear enhancement. **g** Prone image from a CT-guided biopsy of the larger mass, which revealed a lipomatous lesion with prominent myxoid changes